Characteristics of Mesoscale Eddies in the Kuroshio–Oyashio Extension Region Detected from the Distribution of the Sea Surface Height Anomaly

SACHIHIKO ITOH AND ICHIRO YASUDA

Ocean Research Institute, University of Tokyo, Tokyo, Japan

(Manuscript received 2 April 2009, in final form 28 September 2009)

ABSTRACT

This study investigates the distribution of the sea surface height anomaly (SSHA) with the aim of quantifying the characteristics of mesoscale eddies in the Kuroshio–Oyashio extension region (KOER), where intense mesoscale eddies are commonly observed during hydrographic surveys. Dense distributions of both anticyclonic eddies (AEs) and cyclonic eddies (CEs) are detected for the first time in KOER with sufficient temporal and spatial coverage, using the Okubo–Weiss parameter without smoothing. Their contribution to the total SSHA variance is estimated to be about 50%. The zones of highest amplitudes are located north and south of the axis of the Kuroshio Extension (KE) for AEs and CEs, which represent warm-core and cold-core rings, respectively; the areas extend poleward along the Japan and Kuril–Kamchatka Trenches, especially for AEs. Eddies of both polarities and with moderate amplitudes are also recognized along the Subarctic Front (SAF). Eddies in areas north and south of the KE generally propagate westward, at a mean rate of 1–5 cm s^{-1}; those along the trenches south of 46°N and along the SAF propagate poleward at mean rates of 1–2 and 0.5–1 cm s^{-1}, respectively. Because of the asymmetric distribution of the AEs and CEs in the areas north and south of the KE, and the asymmetric amplitude of them along the Japan and Kuril–Kamchatka Trenches, there exist significant eddy fluxes of vorticity, heat, and salinity in these areas.

1. Introduction

The Kuroshio and Oyashio, the western boundary currents of the subtropical and western subarctic gyres of the North Pacific, respectively, separate from the continental shelf to form a region of confluence east of Japan (Fig. 1). The Kuroshio–Oyashio extension region (KOER), defined here as the region encompassing the Kuroshio Extension (KE) and the Oyashio and its extension (also interpreted as return flow) to the east, contains various types of mesoscale eddies with characteristics that indicate an origin from the KE, the Oyashio, the Tsugaru Warm Current (TWC), and the Okhotsk Sea (e.g., Kawai 1972; Yasuda 2003). The eddies may persist in this region for periods ranging from several months to more than one year, and their occurrence and physical and biological evolution have a strong influence on the local climate, hydrography, and fisheries (Sugimoto and Tameishi 1992; Yasuda et al. 1992).

The occurrence and behavior of these mesoscale eddies are known to be related to both bottom topography and variability in currents (e.g., meanders of the KE, southward intrusions and the eastward extension of the Oyashio, and volume fluctuations in the outflows of the TWC and the Okhotsk seawater; Fig. 1c). They are monitored mainly via hydrography, infrared imaging, and altimetry data (Kawai 1972; Yasuda et al. 1988; Shimizu and Ito 1996; Ito and Shimizu 1997; Sainz-Trápaga et al. 1998; Iwao et al. 2003; Yasuda 2003; Isoguchi et al. 2006).

Based on the descriptions and notation provided in previous studies (Iwao et al. 2003; Yasuda 2003), in the present study we refer to bands of relatively high mean northeastward geostrophic velocities corresponding to the extension of the Oyashio and a frontal zone along 40°N as the Subarctic Front (SAF) and Subarctic Boundary (SAB), respectively (Fig. 1). Although the Kuroshio bifurcation front (KBF)—which is considered to bifurcate from the KE near the Shatsky Rise around 160°E to extend northeastward to merge with the SAB—is commonly considered a quasi-stationary hydrographic feature (Sainz-Trápaga et al. 2001; Yasuda 2003), it is not possible to specify its location with reference to the mean geostrophic flow field.

Corresponding author address: Sachihiko Itoh, Ocean Research Institute, University of Tokyo, 1-15-1 Minamidai, Nakano-ku, Tokyo 164-8639, Japan.
E-mail: itohsach@ori.u-tokyo.ac.jp

DOI: 10.1175/2009JPO4265.1

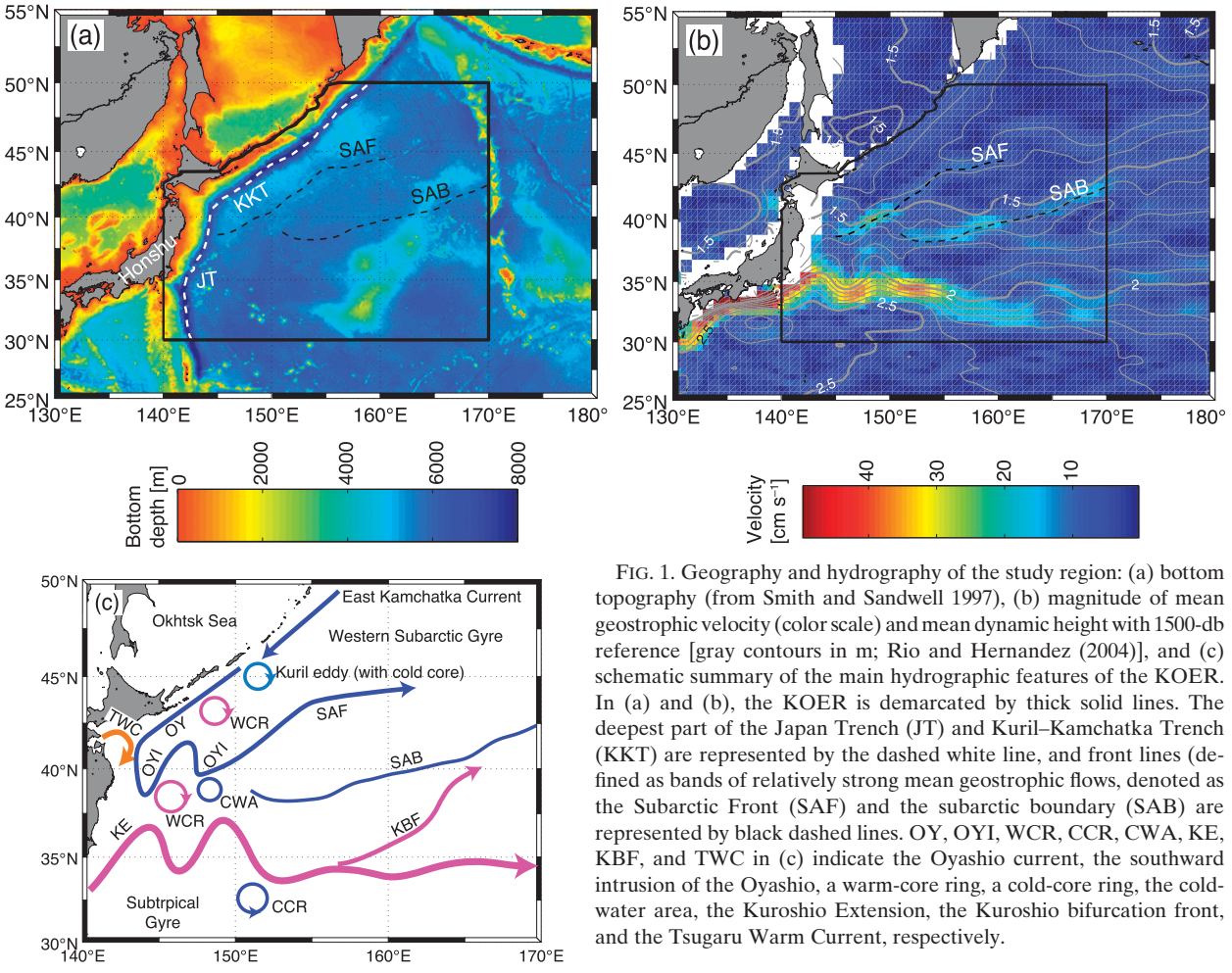

FIG. 1. Geography and hydrography of the study region: (a) bottom topography (from Smith and Sandwell 1997), (b) magnitude of mean geostrophic velocity (color scale) and mean dynamic height with 1500-db reference [gray contours in m; Rio and Hernandez (2004)], and (c) schematic summary of the main hydrographic features of the KOER. In (a) and (b), the KOER is demarcated by thick solid lines. The deepest part of the Japan Trench (JT) and Kuril–Kamchatka Trench (KKT) are represented by the dashed white line, and front lines (defined as bands of relatively strong mean geostrophic flows, denoted as the Subarctic Front (SAF) and the subarctic boundary (SAB) are represented by black dashed lines. OY, OYI, WCR, CCR, CWA, KE, KBF, and TWC in (c) indicate the Oyashio current, the southward intrusion of the Oyashio, a warm-core ring, a cold-core ring, the cold-water area, the Kuroshio Extension, the Kuroshio bifurcation front, and the Tsugaru Warm Current, respectively.

The distribution of anticyclonic warm eddies that originate from the KE (commonly referred to as Kuroshio warm-core rings) is concentrated along the Japan and Kuril–Kamchatka Trenches (hereafter referred to as ''the trenches''), with the eddies showing slow northward movement along the Japan Trench and northeastward movement along the Kuril–Kamchatka Trench (Kitano 1975; Inagake 1997). This pattern was also reported by Hata (1974), Yasuda et al. (1992), and Mishra et al. (1999), who conducted successive hydrographic observations of long-lived warm-core rings from the KE with durations of more than one year. These studies also described intraannual fluctuations in eddy movement caused by interactions with the Oyashio, KE, and other warm eddies.

In analyses of subsurface (at 100-m, 200-m, and 400-m depth) monthly temperature maps compiled by objective analyses of hydrographic data obtained in the area offshore from eastern Japan (Shimizu and Ito 1996; Ito and Shimizu 1997), several anticyclonic warm-core rings (WCRs) are usually recognized in the Kuroshio–Oyashio transition area, typically west of 146°E. Although most of the anticyclonic eddies in the area east of Japan are considered to have originated from the KE or TWC (and hence have warm cores), some that occur in the western subarctic gyre (WSAG) have cold, fresh core water derived from the Okhotsk Sea. The structure and evolution of these so-called Kuril eddies, as detected by hydrographic observations, have been reported previously by Yasuda et al. (2000) and Rogachev (2000).

While the results of numerical experiments suggest that the northward movement of anticyclonic eddies along the trenches is driven by the image effect of a steep slope (Yasuda et al. 1986; Itoh and Sugimoto 2001), the pseudo β effect (caused by a deep poleward current along the slope) has also been proposed as a possible mechanism (Yasuda et al. 2000). Alternatively, Isoguchi and Kawamura (2003) suggested the dominant effects of advection of the Oyashio on the movement of Kuril eddies, which show behavior related to variations in wind-driven transport.

Based on an analysis of temperature distributions at 300-m depth around the KE area obtained from hydrographic observations over the period 1976–80, Mizuno and White (1983) identified 16 WCRs and 9 cold-core rings (CCRs) that were traceable for more than three seasons and were regarded to have anticyclonic and cyclonic polarities, respectively. These WCRs and CCRs were found to occur north and south of the KE axis, respectively. The rings generally moved westward with an average speed of 1 cm s^{-1}, roughly consistent with both the movement pattern and speed of Rossby waves. Northward and southward displacements were commonly found for WCRs and CCRs, respectively, although this is the opposite pattern to that found for isolated eddies in numerical experiments (McWilliams and Flierl 1979).

Cyclonic CCRs are commonly recognized south of the KE in subsurface temperature maps compiled for the area east of Japan. In the area north of the KE, however, it is more common to observe the so-called cold cores or cold-water areas (CWAs) that form near the intrusions of the Oyashio (Kawai 1972; Murakami 1994; Shimizu and Ito 1996; Ito and Shimizu 1997), which are expected to have relatively weak cyclonic polarity. Unlike the occurrences of the two types of anticyclonic eddies (with warm core water or cold core water), there have been no reports of cyclonic WCRs in the KOER.

The Tsugaru warm current develops an anticyclonic gyre in autumn (gyre mode), when a high volume transport of outflow from the Tsugaru Strait occurs, and flows southward along the coast in spring (coastal mode), when outflow is minor (Conlon 1982). The gyre structure often collapses and occasionally shows cyclonic flows over short periods of 20–30 days (Yasuda et al. 1988).

As stated above, previous studies have reported some of the basic characteristics of mesoscale eddies in the KOER (e.g., Mizuno and White 1983). The frequent occurrence and movements of eddies with characteristic core waters, as described in these earlier studies, suggest that they play important roles in the transport of heat, materials, and biota. However, a general and quantitative description of their distribution and movement, which is necessary for assessing the influence of the eddies on transport processes, has yet to be provided, mainly because of the difficulty involved in the detection and tracking of individual eddies using hydrographic and/or infrared images.

Merged sea surface height (SSH) data from the Ocean Topography Experiment (TOPEX)/Poseidon (T/P) and *European Remote Sensing Satellites-1* and *-2* (*ERS-1/2*) or *Jason-1* and *Envisat* altimeters, which have been available since 1993, have sufficient temporal and spatial resolution to enable the detection and tracking of mesoscale eddies. Using these altimetric data in combination with high-resolution sea surface temperature data, Isoguchi et al. (2006) successively described the complex frontal structure of the KOER. A key finding of this earlier study was the detection of two quasi-stationary jets (J1 and J2) that generally formed along bathymetric contours. The positions of J1 and J2 roughly coincide with the SAF and KBF, indicating their important role in the poleward transportation of warm water; however, as the authors mainly focused on quasi-stationary structure, the behavior of individual eddies was not examined.

Isern-Fontanet et al. (2003, hereafter I03) provided a practical procedure for the detection of eddies using the Okubo–Weiss parameter W (Okubo 1970; Weiss 1991) derived from SSH anomaly (SSHA) data; this parameter indicates the relative importance of rotation versus deformation. Using this procedure, Isern-Fontanet et al. (2006, hereafter I06) detected about 20 000 anticyclonic and cyclonic eddies in 213 SSHA maps of the Mediterranean Sea and tracked more than 400 individual anticyclonic and cyclonic eddies.

The same procedure was employed by Chelton et al. (2007, hereafter C07), who examined mesoscale variability in the global ocean via approximately 30 000 individual cyclonic and anticyclonic eddies with lifetimes of $\geq$4 weeks, as detected from 10 years of SSHA data. The authors reported westward propagation of the eddies with a phase speed similar to that of the baroclinic Rossby wave, and slight poleward and equatorward movement of cyclonic and anticyclonic eddies, respectively, consistent with the findings of previous studies on isolated eddies (e.g., McWilliams and Flierl 1979). However, C07 did not describe in detail the variability in eddies near boundary regions, including the KOER where, despite the detection of large numbers of mesoscale eddies via hydrographic observations, there occurs a relatively small number of eddies that make a small contribution to the total SSH variance (typically $\leq$25%) (Fig. 3 in C07). The authors attributed this low detectability to the contribution of short-lived eddies, the properties of the eddy-tracking algorithm, and physical processes other than eddies. However, we consider this low detectability of eddies in the KOER to reflect the low-pass filtering conducted by C07 on the SSHA and W maps, which eliminates relatively small-scale eddies near strongly hyperbolic areas (those areas where deformation dominates rotation).

In the present study, therefore, the characteristics of eddies in the KOER are studied using merged sea surface height data from altimeters, as used in previous studies such as I06 and C07, but without low-pass

filtering prior to the detection of eddies. The main objective of this study is to provide a general and quantitative description of the characteristics of mesoscale eddies in the KOER, which is necessary for assessing the role of eddies in the transport of heat, materials, and biota. The descriptions focus on the following properties of eddies: density (number per unit area), intensity, size, age, and propagation speed, as in previous studies (e.g., Chelton et al. 2007), and associated vorticity and elevation fluxes that are directly related to transport processes. These properties are also required for studies on the dynamics of such eddies.

The remainder of the manuscript is organized as follows. Section 2 provides details on the specifications of SSHA data, methods employed in detecting and tracking eddies, and definitions of eddy properties. The distributions of various eddy properties, trajectories, and fluxes caused by propagation are presented in section 3. Finally, in section 4 the results obtained from SSHA data are compared with previous hydrographic observations, and the general characteristics of mesoscale eddies are given, along with a discussion on their implications for intergyre heat transport and water mass exchange.

2. Data and methods

a. Sea surface height anomaly maps

Gridded SSHA maps calculated from the deviation from the 7-yr mean for the period 1993–99, constructed by merging two sets of source data (T/P and *ERS-1/2* or *Jason-1* and *Envisat* satellite altimeters), were produced by Segment Sol Multimissions d'Alimétrie, d'Orbitographie et de Localization Precise/Data Unification and Altimeter Combination System (Ssalto/Duacs) and distributed by Archiving, Validation and Interpretation of Satellites Oceanographic Data (AVISO), with support from the Centre National d'Etudes Spatiales (CNES) (Ducet et al. 2000; Le Traon et al. 2003; Pascual et al. 2006; AVISO 2008). The maps are produced every 7 days and have a spatial resolution of $\frac{1}{3}° \times \frac{1}{3}°$. The maps from October 1992 to February 2008 for the region 25°–55°N, 130°E–180° are used in the present study in the detection and tracking of eddies. Herein, Rio05 refers to absolute dynamic topography referenced at 1500 db (Rio and Hernandez 2004), as produced by the Collecte Localisation Satellites (CLS) Space Oceanography Division. Bottom topography from Smith and Sandwell (1997) was used in mapping eddy characteristics.

b. Detection and tracking

The procedure employed in this study is basically the same as that used in I03, I06, and C07: areas with a negative value of the Okubo–Weiss parameter, $W = 4[(\partial u/\partial x)^2 + (\partial v/\partial x)(\partial u/\partial y)]$, and less than a critical value W_0 in a geostrophic velocity anomaly map were considered to be eddy areas, and the nearest eddies within a range r in successive maps were regarded as being the same eddy. We adopted $W_0 = -2 \times 10^{-12}$ s^{-2} (following C07) and $r = 100$ km (following I06). In cases when more than two eddies in an earlier map correspond to a single eddy in the subsequent map, the eldest of the two is selected to continue, as employed in C07. Although it has been suggested that some WCRs are absorbed into the KE and then shed from it after a certain time (Tomosada 1986), such regeneration was not considered in the present study because the relevant processes cannot be fully resolved solely from SSHA maps; hence, once an eddy disappeared in a map, it was considered to be terminated and distinct from any eddy that subsequently appeared, even those that appeared at the location where the earlier eddy had been terminated.

Although I03, I06, and C07 applied spatial and temporal low-pass and median filters to SSHA and W maps to extract robust signals, we chose not to use these filters because we consider variability in relatively small-scale eddies located near strongly hyperbolic areas (where deformation dominates rotation) with large positive W, possibly in the frontal area of the KE and the Oyashio, so as to avoid data loss near the lateral boundary. However, the following two requirements for profiles of individual eddies detected based on W maps, as considered in C07, were also assigned in the present study: 1) the eddy should occupy at least four grid boxes with values less than W_0, which represents an equivalent radius approximately equal to the first baroclinic Rossby radius of deformation, about 30 km in KOER (Chelton et al. 1998), and 2) the eddy should have a lifetime greater than $T_0 = 4$ weeks (eddies detected only once are regarded to have a lifetime of 0 weeks). These two conditions were employed to eliminate fluctuations other than eddies, without reducing detectability.

In distinguishing anticyclonic eddies from cyclonic eddies, I03 considered the sign of vorticity in the eddy areas, whereas C07 considered the sign of the SSH anomaly. We chose the former approach because the use of SSHAs without adequate filtering leads to an erroneous interpretation of the polarity due to signals of steric variability; however, most of the detected AEs (CEs) generally have positive (negative) SSHA except for those with extremely small amplitudes. Detection and tracking were conducted for the entire region 25°–55°N, 130°E–180° although detailed analyses were restricted to the northwestern part of the North Pacific (30°–50°N, 140°–170°E) corresponding to the KOER—herein referred to as the study region (Fig. 1). The

region outside of the KOER but within the analysis region of 25°–55°N, 130°E–180° is referred to as the surrounding region.

c. Estimation of eddy properties

The geographical characteristics of eddy properties are investigated based on overlapping 1° × 1° bins centered on the ⅓° × ⅓° grids of the SSHA maps. In terms of basic properties, we estimated the following: cumulative number of anticyclonic eddies (N_A) and cyclonic eddies (N_C), ensemble means of the vorticity amplitude (Z_A and Z_C, maximum of the absolute values of relative vorticity; herein, the subscripts A and C denote anticyclonic and cyclonic), radius (R_A and R_C, where $R = [(\text{area of an eddy})/\pi]^{1/2}$), proportion of eddies older than (based on instantaneous ages) 12 weeks (P_A and P_C; not mean lifetime; first detection is considered as age 0), and propagation speed (U_A, V_A and U_C, V_C, where U and V indicate eastward and northward components, respectively).

In addition to the above basic properties, Eulerian mean fluxes of relative vorticity and SSHA were also estimated:

$$(\overline{u'\zeta'}, \overline{v'\zeta'}) = \frac{1}{T_{\text{obs}} A_{\text{bin}}}\left(\sum(U_A\Gamma_A + U_C\Gamma_C), \quad \sum(V_A\Gamma_A + V_C\Gamma_C)\right), \tag{1}$$

and

$$(\overline{u'\eta'}, \overline{v'\eta'}) = \frac{1}{T_{\text{obs}} A_{\text{bin}}}\left(\sum(U_A\Lambda_A + U_C\Lambda_C), \quad \sum(V_A\Lambda_A + V_C\Lambda_C)\right), \tag{2}$$

where $\sum$ was conducted over all eddies detected in the corresponding bin and T_{obs}, A_{bin}, Γ_A (Γ_C), and Λ_A (Λ_C) indicate the observation period, the area of the bin, area-integrated relative vorticity, and area-integrated SSHA of the AEs (CEs), respectively. The vorticity flux was calculated not only because it influences large-scale ocean circulation (Verron and Le Provost 1991), but also because the method of eddy detection employed in the present study is based on vorticity. Although the distribution of SSHAs is generally negatively related to that of vorticity, the elevation flux was also calculated because it represents a proxy for heat flux. Assuming a negligible barotropic component, the elevation flux can be expressed in terms of heat and salinity fluxes:

$$\begin{aligned}\overline{u'\eta'} &= \overline{u'\int \delta\, dp} \cong \overline{u'\int [\alpha_T T' - \alpha_S S']\, dp} \\ &= \frac{\alpha_T}{\rho_0 C_p}\overline{u'q'} - \alpha_S \overline{u'S'},\end{aligned} \tag{3}$$

where δ, α_T, α_S, T', ρ_0, C_p, $\overline{u'q'}$, and $\overline{u'S'}$ are the volume anomaly of the eddies, thermal expansion coefficient, saline contraction coefficient, temperature anomaly of the eddies, reference density, heat capacity, heat flux, and salinity flux, respectively.

To satisfy the condition of a minimum lifetime of four weeks, all of the above properties were estimated excluding the data for the first and last 4-wk periods, and P_A and P_C were estimated excluding the data of the first and last 12-wk periods.

3. Results

a. Detected eddies and their contribution to SSH variance

This subsection demonstrates the validity of the eddy-detecting method employed in this study. We first present the sensitivity of the three conditions (i.e., $W < W_0$, minimum eddy area of four grid boxes, and minimum lifetime of four weeks) to the SSH variance (roughly proportional to eddy potential energy) step by step, and then show the distribution of the detected eddies on a concurrent sea surface temperature map.

While the number of detected eddies increases with decreasing W_0, their contribution to the total SSH variance asymptotically approaches 55.5%. Using the selected value of $W_0 = -2 \times 10^{-12}$ s^{-2} (following C07), the SSH variance in eddy areas with $W < W_0$ reproduced 54.1% of the total SSH variance—97.4% of the asymptotic value (Fig. 2a). Although the number of detected eddies increased by about 14% with a smaller value of W_0 ($=-2 \times 10^{-13}$ s^{-2}), their contribution to the total SSH variance showed only a slight increase to 55.4%, indicating an increase in subtle signals. We therefore concluded that the selected value of W_0 ($=-2 \times 10^{-12}$ s^{-2}) was low enough to detect most of the mesoscale eddies that were commonly observed to show large variability in the KOER.

After applying the requirement of a minimum of four grid boxes in defining eddy areas, the contribution of the eddies to SSH variance showed a slight decrease to 52.1% of the total variance. After eliminating eddies with lifetimes of $T < T_0 = 4$ wk, the contribution of

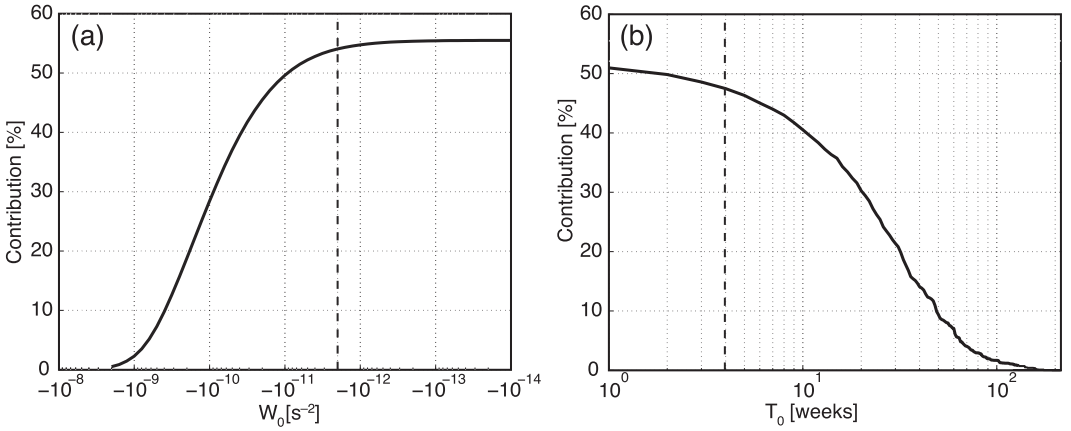

FIG. 2. Contribution to the total SSHA variance of (a) eddy areas with Okubo–Weiss parameter $W < W_0$ and (b) eddies with lifetimes longer than T_0 (weeks). Vertical dashed lines indicate threshold values employed in our analysis; W_0 and T_0 indicate the threshold value of W and threshold value of the eddy lifetime, respectively.

detected eddies was 47.5% (Fig. 2b), which is markedly higher than the estimation reported by C07 (Fig. 4 in C07 shows values in the KOER that are apparently less than 25%). For T_0 = 12 wk, the detected eddies still contained 38.4% of the total variance. In contrast to this moderate decrease in eddy SSH variance (from 54.1% to 47.5%) following the processing described above, the number of eddies fell by one-third, indicating the effective exclusion of erroneous signals.

Figure 3 shows the distributions of AEs and CEs detected from a SSHA map for 26 December 2007 overlaid on an optimally interpolated sea surface temperature (OISST) (Donlon et al. 2002) map for the corresponding period (mean values for the period from 23 to 29 December). The detected AEs and CEs that met all the requirements stated above (as plotted using black symbols), except for those near the Kuril Islands, were located on the crests and troughs of OISSTs, which generally correspond to maxima and minima in subsurface temperature maps, respectively. This finding demonstrates the validity of the eddy-detecting method employed in the present study, even for the frontal area. While the AEs were frequently detected in the troughs of OISST near the Kuril Islands (Fig. 3a), their origin is attributed to anticyclonic cold-core rings, as reported in previous studies (Rogachev 2000; Yasuda et al. 2000).

We ultimately identified about 4400 AEs and 4700 CEs, and tracked them in the study region of the KOER during the available period of 790 weeks (about 16 years and 2 months).We found 1659 (155) AEs and 913 (144) CEs with lifetimes ≥12 wk (52 wk). The cumulative numbers were approximately 59 000 for AEs and 63 000 for CEs, indicating an average of 75 AEs and 80 CEs observed in the study region each week.

b. Basic properties

1) NUMBER OF EDDIES

Figure 4 shows the distribution of the density (total number detected in a 1° × 1° bin) of anticyclonic and

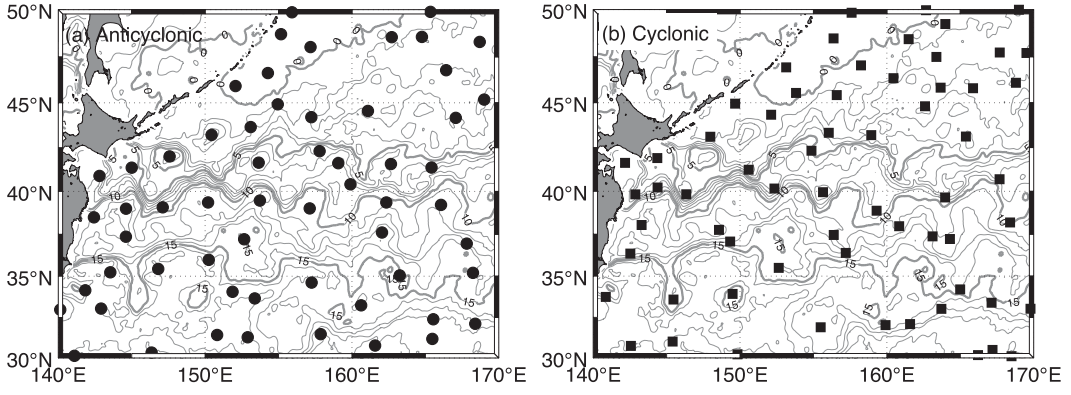

FIG. 3. Distribution of detected (a) anticyclonic and (b) cyclonic eddies (black symbols) from an SSHA map for 26 Dec 2007 overlaid on a map of OISST [in °C; gray contours; Donlon et al. (2002)] for the same period.

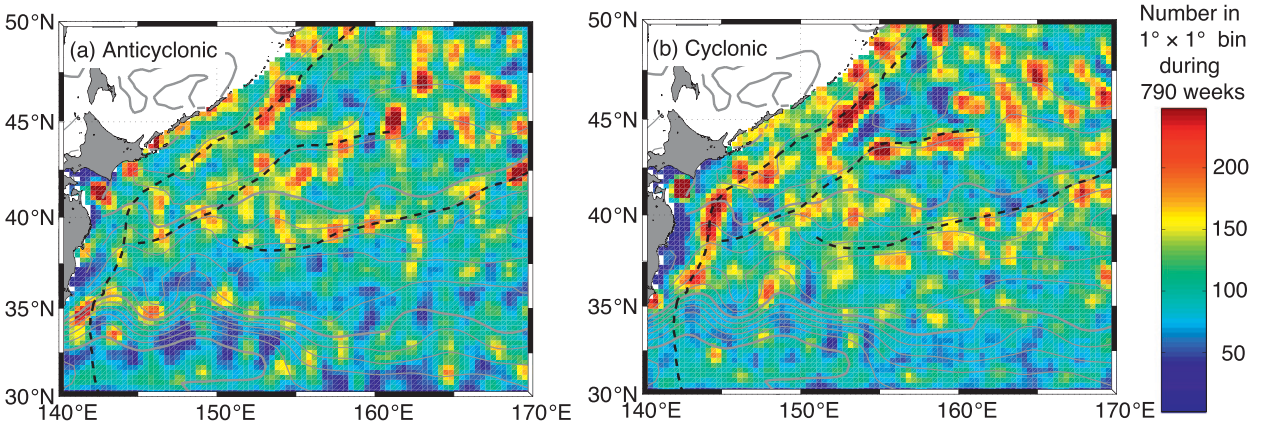

FIG. 4. Distribution of the number of (a) anticyclonic and (b) cyclonic eddies (N_A and N_C, respectively) detected in 1° × 1° bins during the analysis period of 790 weeks. The deepest part of the trenches, the SAF, and the SAB are shown by dashed lines, and gray contours show the mean dynamic height, as in Fig. 1. Values larger than 250 are shown with the same color as that assigned to a value of 250.

cyclonic eddies (N_A and N_C, respectively) during the observation period. Dense areas of $N_A > 150$ and $N_C > 150$ occur locally along the trenches; the northern and southern flanks of the KE, SAF, SAB; and along the TWC. The maximum values ($N_A = 335$ and $N_C = 442$) were observed in the area of the TWC. AEs were more frequently observed along the northern flank of the KE than were CEs, but less frequently observed along the southern flank. CEs were more densely distributed along the trenches than were AEs. The patchy distribution of high-density areas is attributable to high frequency occurrences of eddies in the same locations corresponding to the geography and quasi-stationary hydrographic features, and characteristic horizontal scales of eddies (radius distributions are presented later).

2) VORTICITY AMPLITUDE

The mean vorticity amplitude (Z_A and Z_C) was highest around the KE, especially in its western part, with high values extending slightly along the trenches (Fig. 5). A detailed analysis of the data reveals several differences between Z_A and Z_C: Z_A was higher than Z_C in the TWC area and along the trenches; the zone of highest Z_A was located upon or north of the axis of the KE, whereas the zone of highest Z_C was located upon or slightly south of the axis. The amplitude of AEs decreased along the trenches from 35° to 43°N, although an area of elevated values occurs around 46°–47°N. An area of relatively high amplitude observed along the trenches around 50°N appears to be related to an area farther north, outside of the KOER. The maximum amplitude of AEs (3×10^{-5} s^{-1}) occurred on the northern flank of the KE, smaller than the maximum amplitude of CEs found on the southern flank (5×10^{-5} s^{-1}). For both Z_A and Z_C, the amplitude was slightly enhanced along the SAF.

3) RADIUS

Large values of mean radii (R_A and R_C) were observed around the KE south of the SAB. The difference in the distribution patterns of R_A and R_C is more pronounced

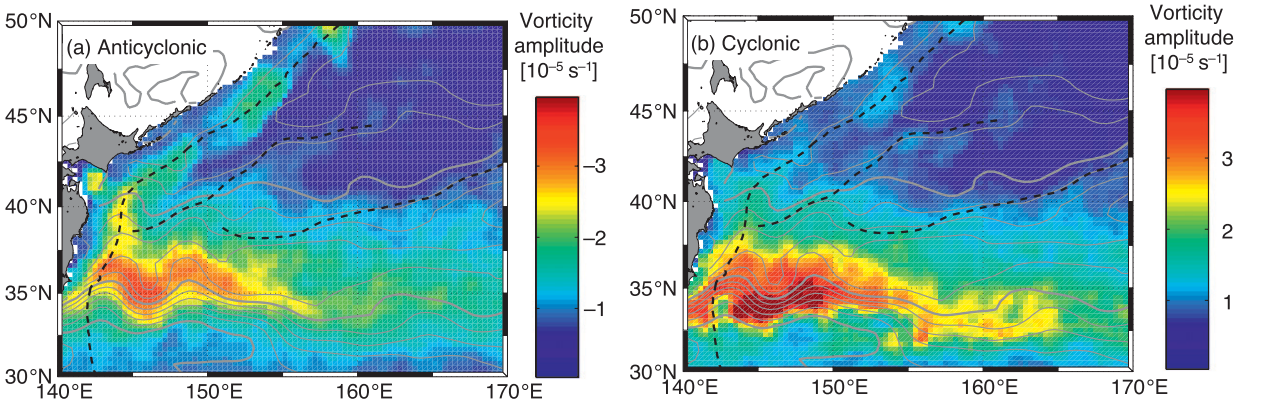

FIG. 5. As in Fig. 4, but for ensemble-mean vorticity amplitude, Z_A and Z_C.

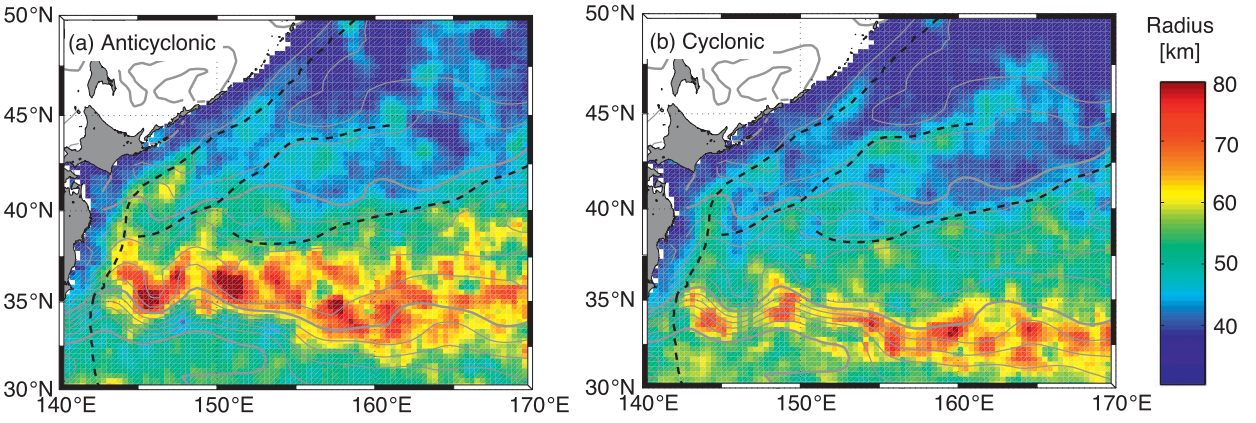

FIG. 6. As in Fig. 4, but for eddy radii (km), R_A and R_C.

than that for the vorticity amplitude (i.e., Z_A versus Z_C; Fig. 6). Large values of R_A, typically exceeding 60 km, are clearly observed in the area north of the KE, while large values of R_C occur along the axis of the KE. For both polarities, areas of relatively large radii were recognized along the trenches and southern margin of the SAF. The maximum value of R_A (89 km) was found at the first trough of the KE (at 145°20′E), while the maximum value of R_C (80 km) occurred along the KE at ~160°E.

4) AGES OF EDDIES

The proportion of eddies older than 12 weeks (P_A and P_C) is shown in Fig. 7. Higher concentrations of old AEs ($P_A \geq 50\%$) were recognized along the trenches, SAF, and SAB. Values along the trenches and the eastern part of the SAB (northern part of the KBF) exceeded 80%, but were extremely low (less than 20%) south of the KE. A similar pattern was observed for CEs, although with smaller values along the trenches and in the area between the KE and SAB, and with larger values in the areas around the TWC and the eastern part of KE. Because P_A and P_C simply represented the relative frequency of old (≥12 wk) eddies to all eddies, high (low) values could either reflect frequent (infrequent) occurrences of old eddies or infrequent (frequent) occurrences of young eddies. The distributions of P_A and P_C are also compared with the trajectories of long-lived eddies in the following subsection.

c. *Propagation and associated flux*

1) PROPAGATION

Figure 8 shows the mean propagation speeds of detected eddies. For both AEs and CEs, westward propagation is clearly observed in zones north and south of the KE and in an eastern KE area (east of 160°E). Propagation speeds were 1–2 cm s^{-1} in the zone north of the KE and 1–5 cm s^{-1} in the zone south of the KE and the eastern KE area. Zonal propagation was not evident in the KE area west of 160°E, where the mean eastward geostrophic flow exceeds 20 cm s^{-1} (Fig. 1b); instead, we found southward movement of CEs around the first two troughs and northward movement of AEs around the first two crests, both across the contour lines

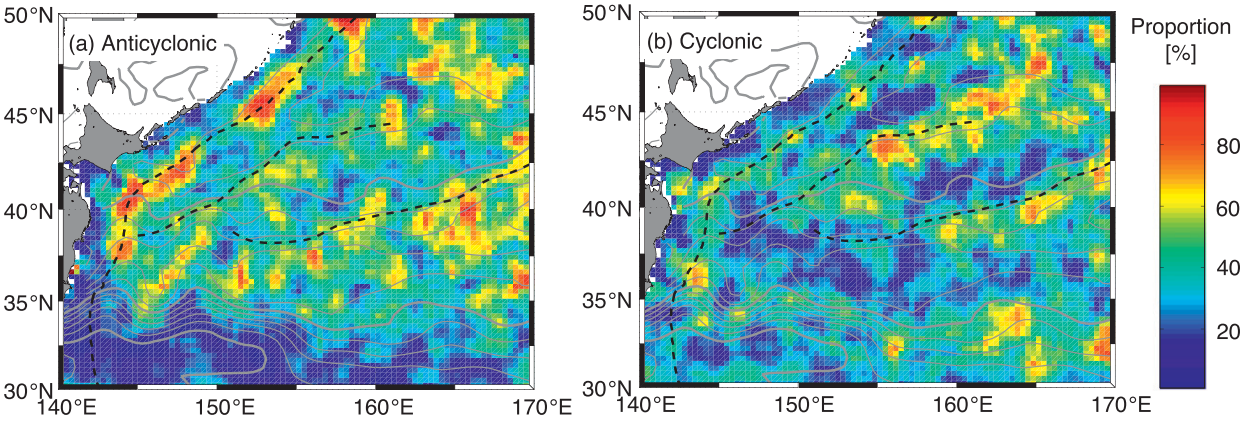

FIG. 7. As in Fig. 4, but for the proportion of eddies (%) with age ≥12 wk, P_A and P_C.

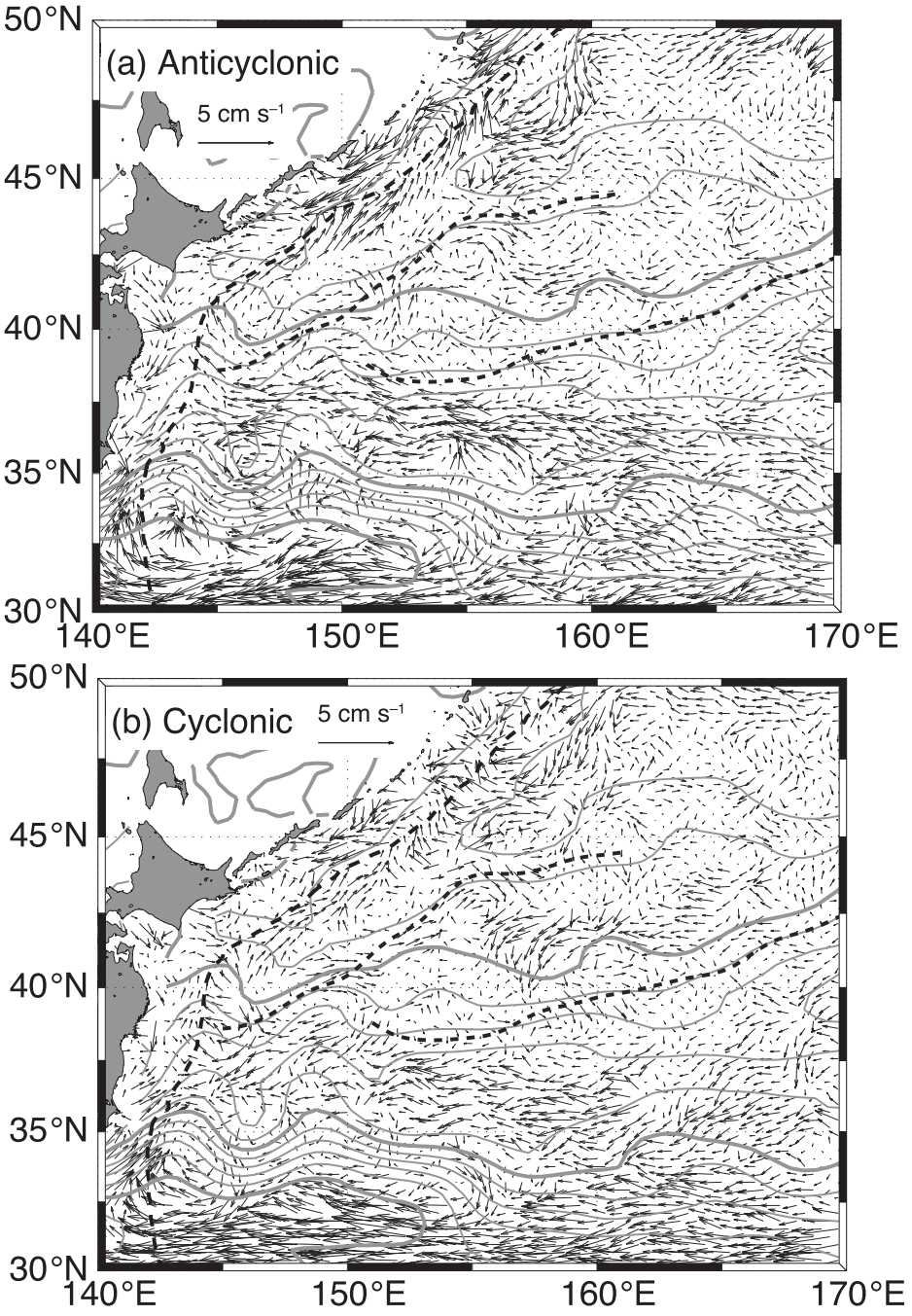

FIG. 8. As in Fig. 4, but for propagation speed (cm s^{-1}), U_A, V_A and U_C, V_C.

of mean dynamic height, which approximately coincide with mean geostrophic streamlines. We observed slow propagation toward the east and northeast along the SAF at rates of 0.5–1 cm s^{-1}. Propagation along the SAB was negligible or very slow to the west.

The most remarkable characteristics of eddy propagation in this region were observed along the trenches and their offshore flanks, where both AEs and CEs moved poleward along the trenches at 1–2 cm s^{-1}. This trend was observed north of approximately 37°N for AEs and north of approximately 40°N for CEs and south of 46°–47°N for both AEs and CEs. At 46°–47°N the northeastward vectors met southwestward vectors from the area to the northeast, and turned northwestward to cross the deepest part of the trenches to the onshore side, where both AEs and CEs showed southwestward

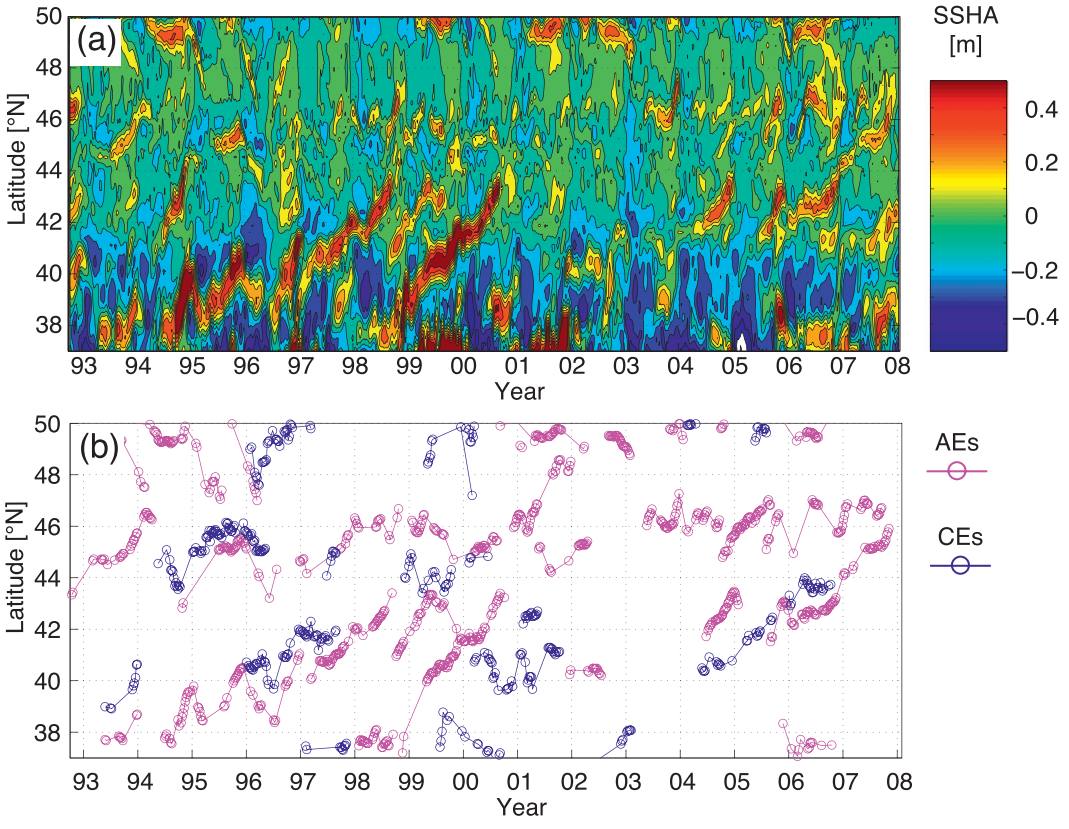

FIG. 9. Temporal variability in (a) SSHA (m) and (b) distribution of long-lived eddies (≥52 wk) along the Japan and Kuril–Kamchatka Trenches for the period 1993–2008. In (b), the time and latitude of eddies within 1/4° from the trenches were plotted, and marks connected with lines for the same eddies.

propagation from the area north of 50°N to about 42°N around the TWC. Farther south, east of Honshu, AEs showed a southward propagation from the TWC along the coast; no such trend was observed for CEs.

To further examine the above characteristics of eddy propagation along the trenches, we investigated the temporal variability in SSHA along the trenches (Fig. 9a), shown with time–latitude plots of long-lived eddies (≥52 wk) distributed along the trenches (Fig. 9b). Northward and northeastward propagation was clearly recognized for positive SSHAs, largely corresponding to occurrences of AEs along the trenches. One of the most prominent signals began in 1993 and reached 43°N by 1998, representing the movement of the so-called WCR 93A (Mishra et al. 1999), although regenerations were not reproduced in the present study. The propagation of negative SSHA showed much smaller amplitudes than those of positive SSHA; relatively strong signals of negative SSHA were found around the prominent positive signals. The change to coastward eddy propagation at around 46°N (see Fig. 8) is also apparent in SSHA variability.

Figure 10 shows the trajectories of eddies with lifetimes ≥52 wk. Although some trajectories occurred in the Okhotsk Sea, the passing of eddies through the straits of the Kuril Islands is not considered in this study, as careful confirmation is required for the employed eddy-detection method (which assumes a quasigeostrophic flow field) when applied to areas of strong tidal flow. The distribution of trajectories is similar to those in Fig. 7, which shows the proportion of eddies aged ≥12 wk. This finding suggests that high P_A and P_C were caused by the occurrences of long-lived eddies.

Long-distance westward propagations (typically exceeding 10° longitude) were observed in the area around the eastern part of the KE and the northeastern area of the WSAG, near the Aleutian Islands. Long-distance propagation of CEs was mostly observed in the KE and on its southern flank, while a number of AEs were found in the areas north and south of the KE, and in the WSAG. Poleward movements along the trenches, exceeding 3° in latitude, were found for AEs, whereas the movements of CEs along the trenches were generally shorter. The origins of the long-lived AEs observed along the trenches were located slightly west of the trenches area, especially for those along the Japan Trench. Although we were able to identify concentrations

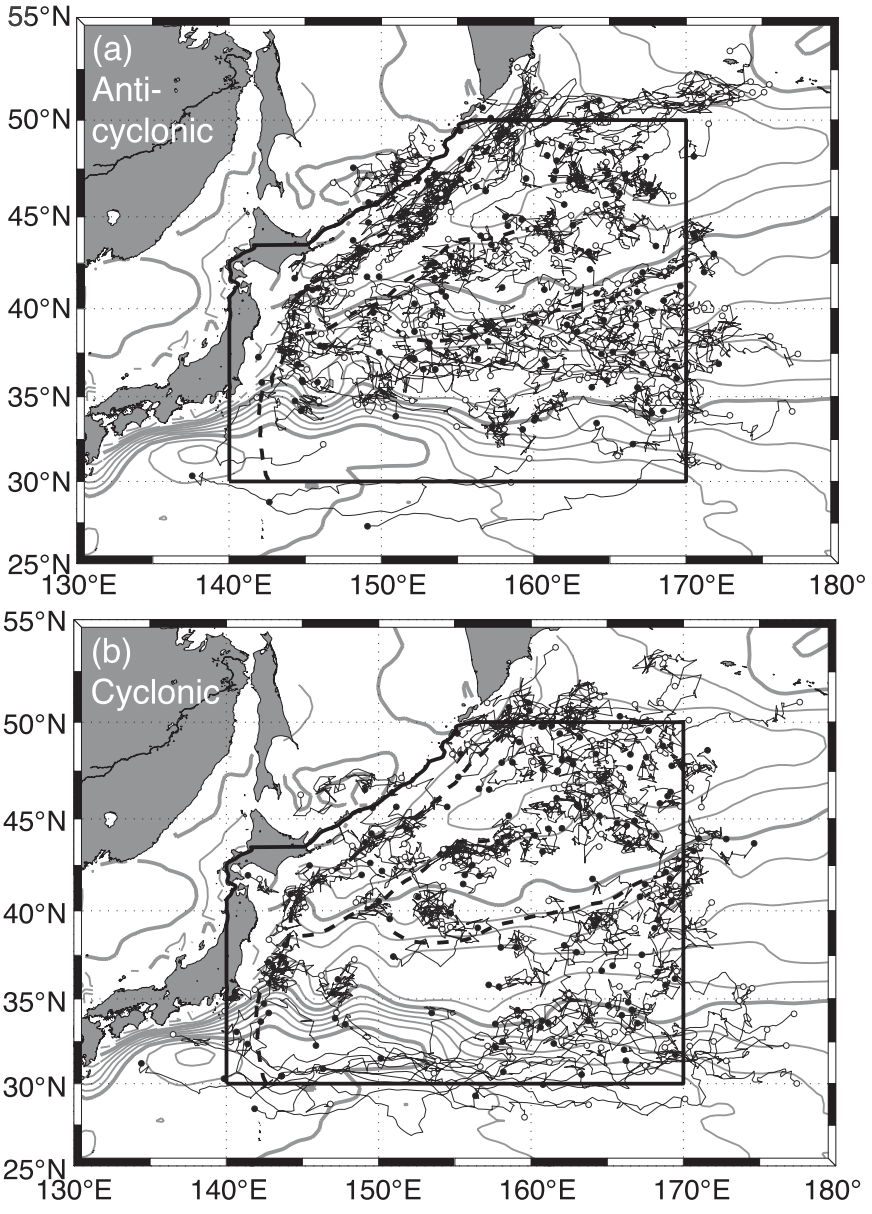

FIG. 10. Trajectories of (a) anticyclonic and (b) cyclonic eddies with lifetimes ≥52 wk. Open and solid circles indicate the start and end points of each trajectory, respectively. The deepest part of the trenches, the SAF, and the SAB are shown by dashed lines; gray contours show the mean dynamic height, as in Fig. 1.

of trajectories, movement along the SAF was not as clearly defined as that along the trenches.

2) VORTICITY AND ELEVATION FLUX

Figure 11 shows the Eulerian mean eddy fluxes of relative vorticity anomalies and SSHAs caused by eddy propagation. The two fluxes have a similar distribution, although with opposite sign. We observed westward (eastward), eastward (westward), and southward (northward) flux of vorticity (elevation) in zones located south and north of the KE and around crests, respectively. Although there occurred localized northward (southward) fluxes in vorticity (elevation), their amplitude and spatial extent were no larger than those of the southward (northward) flux. Zonal integration reveals a minimum (maximum) vorticity (elevation) flux of about -0.035 m s^{-2} (900 m^2 s^{-1}) around 35°N (data not shown). While both CEs and AEs showed poleward movement along the offshore side of the trenches, the total flux of vorticity (elevation) caused by the propagation was equatorward

(poleward), indicating the dominant contribution of AEs. The offshore (onshore) flux of vorticity (elevation) corresponding to the onshore movement of AEs was recognized around 46°–47°N. The fluxes along the onshore sides of the trenches were generally weaker than those along the offshore sides.

4. Discussion

The first part of this section (section 4a) examines the correspondence between eddies detected in SSHA maps and hydrographically observed WCRs and CCRs with relatively large amplitudes. Section 4b describes the general characteristics of mesoscale eddies in the KOER, including decaying eddies in the area distant from the formation region and those distributed a long way east of Japan, where hydrographic observations were too sparse to enable the tracking of eddies. This is the first quantitative description of the characteristics of mesoscale eddies in this region, which has not been resolved in smoothed SSHA maps. Finally, section 4c considers the implications of eddy movement patterns for heat transport and water mass exchange.

a. Detected eddies versus WCRs and CCRs based on hydrographic observations

While several anticyclonic WCRs (including an anticyclonic gyre of the TWC and cyclonic CCRs) are usually found in subsurface temperature maps compiled for the area east of Japan (e.g., Shimizu and Ito 1996; Ito and Shimizu 1997), we detected an average of 75 AEs and 80 CEs in SSHA maps of the KOER, which corresponds to an increase by a factor of 2 or 3 compared with observations from temperature maps, considering that subsurface temperature maps generally cover 5%–10% of the area of the KOER. The number of long-lived eddies identified in the present study (155 AEs and 144 CEs with lifetimes ≥52 wk for 16 years of data) was greater than that reported by Mizuno and White (1983), who found 16 WCRs and 9 CCRs for 4 years of data in the area around the KE (30°–45°N, 130°E–170°W, representing an area approximately 1.5 times larger than the KOER). Although anticyclonic CCRs (with cold but fresh and light core waters) originating from the Okhotsk Sea (Yasuda et al. 2000) were included in the AEs detected from SSHA maps, the fact that these rings were distinguished from WCRs does not explain the above difference, as the number of anticyclonic CCRs across the entire KOER area does not exceed the number of WCRs.

The primary reason for this discrepancy between the present and previous studies is the difference in the amplitude criterion employed in detecting eddies: while previous studies generally recognized eddies if the subsurface temperature amplitude was larger than the critical value of 0.5°–1.0°C, based on closed contour lines, the present study required the Okubo–Weiss parameter W to be less than the critical value of $W_0 = -2 \times 10^{-12}$ s^{-2}. The minimum detectable SSHA amplitude of the present and previous studies, $\Delta\eta_{\text{present}}$ and $\Delta\eta_{\text{previous}}$, respectively, can be estimated as follows:

$$\Delta\eta_{\text{present}} \sim \frac{\sqrt{W_0}}{2}\frac{f}{g}L^2 \tag{4}$$

and

$$\Delta\eta_{\text{previous}} \sim \frac{g'}{g}\Delta h_{\text{previous}} = \frac{g'}{g}\frac{\Delta T_{\text{previous}}}{\partial T/\partial z}, \tag{5}$$

where f, g, g', L, $\Delta h_{\text{previous}}$, $\partial T/\partial z$, and $\Delta T_{\text{previous}}$ denote the Coriolis parameter, acceleration of gravity, the reduced gravity, horizontal scale of the eddies, minimum detectable vertical displacement of the isothermal surfaces, vertical temperature gradient in the subsurface layer, and the temperature amplitude criterion employed in previous studies, respectively. Using typical values in the study region of $f = 10^{-4}$ s^{-1}, $L = 60$ km, $g'/g = 2 \times 10^{-3}$, $\partial T/\partial z = 10^{-2}$ °C m^{-1} (at 200–400-m depth; relatively high values up to about 3×10^{-2} °C m^{-1} along the northern flank of the KE and decreasing northward to become almost zero around 45°N) (Conkright et al. 2002), and $\Delta T_{\text{previous}} = 0.5$°C, we obtain $\Delta\eta_{\text{present}} \sim 2.5$ cm and $\Delta\eta_{\text{previous}} \sim 10$ cm (about 3 cm in the zone north of KE and tens of centimeters north of 40°N). Therefore, the present study detected weaker-amplitude eddies than the previous studies using subsurface temperature maps, especially in the areas distant from the KE.

Considering that WCRs and CCRs defined in the subsurface temperature maps are expected to have relatively strong vorticity amplitudes, we suggest that it is better to compare their distribution with areas of strong mean vorticity amplitude in detected eddies (Fig. 5) rather than with all detected eddies. The high-amplitude zones of AEs and CEs on the northern and southern flanks of the KE are basically consistent with the distribution of WCRs and CCRs in the areas north and south of the KE, respectively. The extension of high-amplitude zones of AEs along the trenches suggests the frequent occurrence of intense WCRs, consistent with the results of previous studies (Kitano 1975; Yasuda et al. 1992; Mishra et al. 1999).

A high concentration of moderate-amplitude (Fig. 5a) CEs along the trenches (Fig. 4a) is probably related to CWAs shed from southward intrusions of the Oyashio,

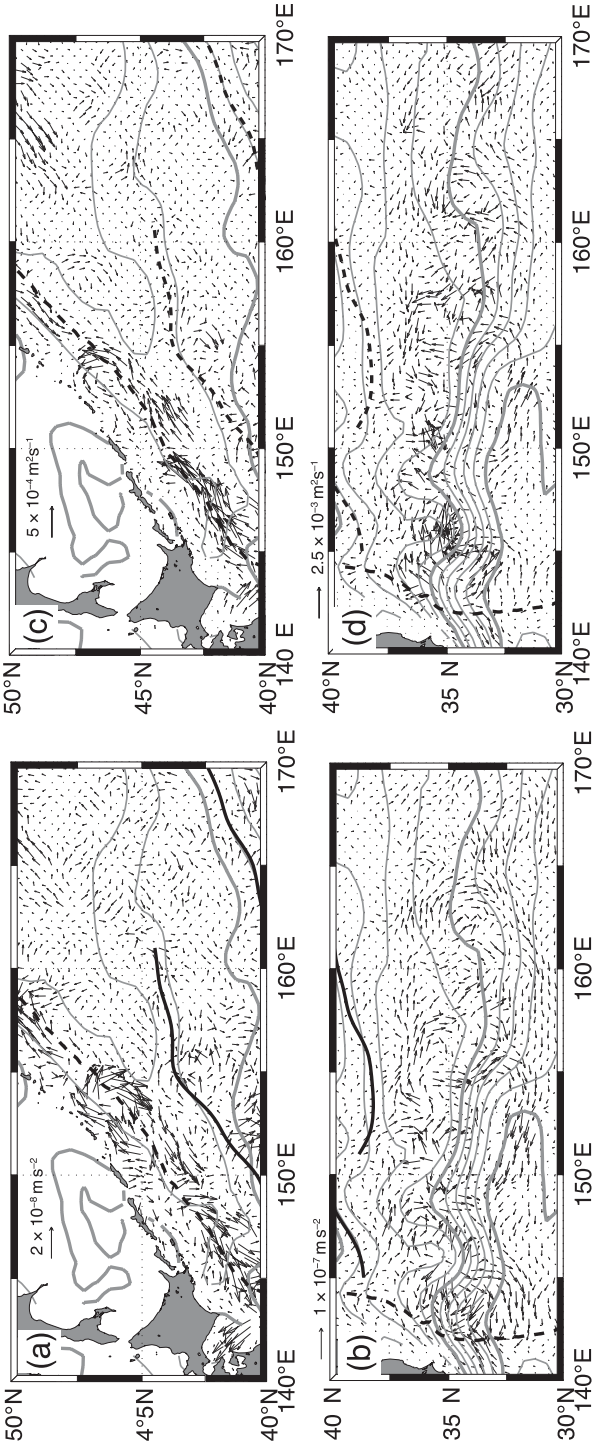

FIG. 11. Distribution of the Eulerian mean flux of vorticity anomalies for the (a) northern and (b) southern areas of the KOER, and the SSHA caused by eddy propagation for the (c) northern and (d), (d) areas of the KOER. The northern and southern areas of the KOER are shown separately because the magnitude of fluxes around the KE in the southern area are much higher than that in the northern area. The deepest part of the trenches, the SAF, and the SAB are shown by dashed lines, and gray contours show the mean dynamic height, as in Fig. 1.

which are frequently observed, although their flow structures are less clear than those found south of the KE. For the TWC area, an anticyclonic gyre was clearly detected as AEs with strong vorticity amplitude (Figs. 4a and 5a), while cyclonic flow observed during the collapse phase of the gyre (Yasuda et al. 1988) was detected as a relatively weak signal (Figs. 4b and 5b). The southward along-coast propagation of AEs is considered to be caused by the transition from the gyre mode to the coastal mode.

The occurrence of large-radius eddies around the KE and along the trenches, similar to the extent of strong-amplitude areas, can be explained if strong WCRs and CCRs are larger than weak AEs and CEs. The observation that the area of large-radius AEs (CEs) extends farther north (south) than the area of strong-amplitude eddies possibly reflects the fact that strong but relatively small-scale frontal fluctuations were included in the detected eddies around the KE axis.

Although the strongest and largest eddies were detected around the KE, a greater number of long-lived eddies was observed in the region north of the KE (Figs. 7 and 10). As mentioned above, it is possible that some of the long-lived eddies might have decayed from their initial stage and were therefore ignored in subsurface temperature maps (if their temperature amplitude was below the typical criteria of 0.5°–1.0°C); however, high-amplitude eddies and a large proportion of old eddies were identified for AEs along the trenches, thereby indicating the occurrence in this area of long-lived AEs with large amplitudes. As is evident in Figs. 8 and 9, these AEs showed a trend to move northward along the trenches, consistent with previous observations of the long-term northward movement along the trenches of intense WCRs that originated from the KE (Hata 1974; Yasuda et al. 1992; Mishra et al. 1999). Based on the amplitude of AE hotspots located around 46°–47°N along the Kuril–Kamchatka Trench, we infer the significant contribution of Kuril eddies generated by outflows of cold Okhotsk seawater, as also suggested by previous hydrographic observations (Rogachev 2000; Yasuda et al. 2000).

b. Characteristics of mesoscale eddies in the KOER

Figure 12 provides a summary of the observed eddy behavior. While large variability in SSH has been noted for the KOER, especially around the KE (Qiu 2002), approximately 50% of the variance is attributable to mesoscale eddies with radii larger than the first baroclinic Rossby radius of deformation and with lifetimes longer than one month. It is considered that a significant contribution to the total variance is made by eddies with a horizontal scale less than 1.5° and those distributed near frontal areas (e.g., of the KE, Oyashio intrusions, and the SAF, where deformation is likely to dominate rotation), as this contribution is approximately twice that calculated by C07, who conducted a 1.5° × 1.5° low-pass filter on W maps.

The observed distribution of the mean amplitude suggests that the strongest mesoscale eddies of both polarities are generated along the KE: anticyclonic WCRs are pinched off from the KE to the north as Kuroshio WCRs, and cyclonic CCRs are formed in the area south of the jet from troughs of the KE with core water that originated from the area north of the KE, probably with properties intermediate between those of the KE and the Oyashio. The WCRs and CCRs then start moving westward due to the planetary β effect. The fact that they do not move eastward despite the mean eastward geostrophic flow can be partly explained by the shear-induced β effect, which is balanced by the geostrophic flow (van Leeuwen 2007); however, because the KE is more complex than the simple background flow, a detailed analysis is required to clarify the relevant mechanism.

In the area near the western end of the KOER, the trajectories and distributions of various properties indicate a major path (along the trenches) and a minor path (along the SAF) driving eddies poleward. Large numbers of intense AEs that formed north of the KE are considered to move poleward along these paths. Although many CEs were also detected along these paths, most of the strong CEs that formed south of the KE are unlikely to be included because the KE jet lies between the eddies and the paths. As discussed in the preceding subsection, the origin of the CEs with relatively weak amplitudes along these paths is likely to be the Oyashio, which intrudes southward and often sheds CWAs. This interpretation is consistent with the propagation characteristics in the area between 37° and 40°N along the Japan Trench, where AEs showed northward propagation but CEs did not (Fig. 8), as the formation of CWAs is related to the southward intrusions of the Oyashio.

As shown in Fig. 9, the prominent SSHA signals moving poleward along the trenches up to 46°N were caused by AEs, supported by fluxes of vorticity and elevation (Fig. 10). The similar movement pattern of CEs observed in Fig. 8 is possibly due to CWAs that were pushed poleward by the intense AEs or weak cyclonic features generated by strong flows around AEs. With poleward movement along the trenches far from the Kuroshio, the AEs appear to lose their vorticity amplitude, as seen in the decrease along the trenches up to about 44°N (Fig. 5a), even though the northward movement supplies negative vorticity from the rotating earth. However, the decreasing trend changed at around 44°N, whereas AEs still showed a mean northeastward movement.

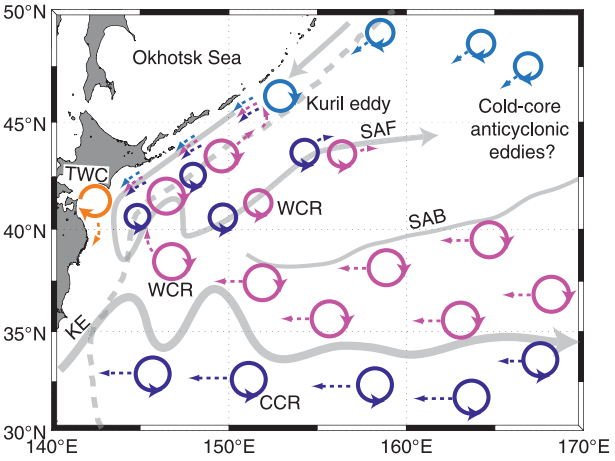

FIG. 12. Schematic summary of the behavior of mesoscale eddies in the KOER. Thin dashed arrows indicate movement directions. Flows of the Oyashio and the KE, the SAF, and the SAB are shown by solid gray lines; the deepest part of the Japan and Kuril–Kamchatka Trenches is depicted by a dashed gray line. WCR, CCR, KE, SAF, SAB, and TWC represent warm-core ring, cold-core ring, the Kuroshio Extension, Subarctic Front, subarctic boundary, and the Tsugaru Warm Current, respectively.

Taking previous hydrographic observations into account (Rogachev 2000; Yasuda et al. 2000), we suggest that the above observation can be explained by the Kuril eddies with cold Okhotsk seawater in their core. Another area of relatively large-amplitude AEs around 50°N may be related to anticyclonic Kamchatka eddies moving southwestward from the Bering Sea (Rogachev et al. 2007). The turning of the northeastward movement to the inshore side of the Kuril–Kamchatka Trench around 46°–47°N suggests vigorous interaction between these different types of AEs, yet the relevant processes cannot be examined solely in terms of SSHA data. Although the southwestward movement of AEs and CEs along the inshore side of the Kuril–Kamchatka Trench is attributable to the southwestward mean geostrophic flow, as suggested by Isoguchi and Kawamura (2003), we have yet to confirm the mechanism of the poleward movement of AEs from the KE along the trenches, for which the pseudo β effect, or the image effect, have been proposed (Yasuda et al. 1986; Yasuda et al. 2000; Itoh and Sugimoto 2001).

Because SAF is considered as an equivalent quasi-stationary jet J1 proposed by Isoguchi et al. (2006), it is possible that the poleward propagation of AEs is partly related to the poleward transport of warm water by J1. In contrast, elevation flux estimates indicate that net eddy heat transport is insignificant along the SAF because the contribution of CEs was approximately equivalent to that of AEs (in contrast to the situation along the trenches). The propagation along the SAF is likely to be related to the mean geostrophic flow, although the propagation speed of 0.5–1 cm s^{-1} is much less than the flow speed, which is O(10 cm s^{-1}). While pairs of AEs and CEs along the northern and southern side of the SAF may drive themselves poleward, the antisymmetric distribution of AEs and CEs cannot be confirmed from the present analyses.

c. *Implications for heat transport and water mass exchange*

Propagating eddies, which result in fluxes of various quantities such as vorticity, heat, and nutrients, are likely to make a significant contribution to the oceanic circulation, biological production, and temporal and spatial variability in these features. Zonal fluxes of vorticity in areas located north and south of the KE axis, arising from westward-propagating AEs and CEs, supply negative and positive vorticity to the western boundary, respectively. This redistribution of vorticity may act to amplify WCRs around the Japan Trench and lead to the decay of the anticyclonic recirculation gyre south of KE.

Although the present study was based solely on vortices detected in SSHA maps and, although the estimated fluxes represented only a part of the total eddy flux, it is interesting to evaluate the fluxes and compare them with previous studies because our technique, based on the eddy propagation speed, is different from the conventional method, based on the correlation between temperature and velocity in Eulerian coordinates. In the case for which density anomalies are solely caused by temperature anomalies, the distributions of heat flux expressed in Eq. (3) are equivalent to those of the elevation flux by the factor $\rho_0 C_p/\alpha_T \sim 2 \times 10^{10}$ J m^{-3}, with $\rho_0 \sim 10^3$ kg m^{-3}, $C_p \sim 4 \times 10^3$ J kg^{-1} K^{-1}, and $\alpha_T \sim 2 \times 10^{-4}$ K^{-1}. Using this scaling, the maximum value of zonally integrated northward elevation flux from 170°E to the western boundary of 900 ± 250 m^2 s^{-1} at around 35°N (as estimated in section 3) is equivalent to a northward heat transport of 0.018 (±0.0005) PW. This is corrected to 0.02–0.03 PW based on the positive relationship between temperature and salinity anomalies in the upper layer of this zone (Suga and Hanawa 1990; Yasuda et al. 1996). Regarding the contribution of the eastern North Pacific, we suggest that the poleward heat flux caused by the movement of eddies is comparable to the total poleward eddy heat flux, including the contribution of noneddy (nonvortex) variability, which was recently estimated to be about 0.1 PW around 30°–40°N based on an ocean general circulation model (Jayne and Marotzke 2002) and analyses of Argo, satellite sea surface temperature, and satellite altimeter data (Qiu and Chen 2005).

While heat transport can occur by both eddies and noneddy fluctuations, significant material transport only occurs via the movement of intense eddies that trap water within their core. Long-distance poleward movements of intense WCRs along the trenches are therefore considered to play an important role in the exchange of salinity and nutrients between the subtropical and western subarctic gyres.

Acknowledgments. The authors are grateful to two anonymous reviewers and the journal editor for their valuable comments. S. Itoh was financially supported by the Japanese Ministry of Education, Culture, Sports, Sciences and Technology [KAKENHI, Grand-in-Aid for Young Scientists (B), 21740340].

REFERENCES

AVISO, 2008: SSALTO/DUACS user handbook: (M)SLA and (M)ADT near-real time and delayed time products. Aviso Altimetry, Ramonville St. Agne, France, 32 pp.

Chelton, D. B., R. A. DeSzoeke, M. G. Schlax, K. El Naggar, and N. Siwertz, 1998: Geographical variability of the first baroclinic Rossby radius of deformation. *J. Phys. Oceanogr.,* **28,** 433–460.

——, M. G. Schlax, R. M. Samelson, and R. A. de Szoeke, 2007: Global observations of large oceanic eddies. *Geophys. Res. Lett.,* **34,** L15606, doi:10.1029/2007GL030812.

Conkright, M. E., R. A. Locarnini, H. E. Garcia, T. D. O'Brien, T. P. Boyer, C. Stephens, and J. I. Antonov, 2002: *World Ocean Atlas 2001: Objective Analyses, Data Statistics, and Figures, CD-ROM Documentation*. National Oceanographic Data Center Internal Rep. 17, 17 pp.

Conlon, D. M., 1982: On the outflow modes of the Tsugaru Warm Current. *Mer (Paris),* **20,** 60–64.

Donlon, C. J., P. J. Minnett, C. Gentemann, T. J. Nightingale, I. J. Barton, B. Ward, and M. J. Murray, 2002: Toward improved validation of satellite sea surface skin temperature measurements for climate research. *J. Climate,* **15,** 353–369.

Ducet, N., P. Y. Le Traon, and G. Reverdin, 2000: Global high-resolution mapping of ocean circulation from TOPEX/Poseidon and ERS-1 and -2. *J. Geophys. Res.,* **105,** 19 477–19 498.

Hata, K., 1974: Behavior of a warm eddy detached from the Kuroshio (in Japanese with English abstract). *J. Meteor. Res.,* **26,** 295–321.

Inagake, D., 1997: Statistics of the Kukroshio warm-core ring migration by historical data from 1981 to July 1996 (in Japanese with English abstract). *Bull. Tohoku Reg. Fish. Res. Inst.,* **59,** 149–162.

Isern-Fontanet, J., E. Garcia-Ladona, and J. Font, 2003: Identification of marine eddies from altimetric maps. *J. Atmos. Oceanic Technol.,* **20,** 772–778.

——, ——, and ——, 2006: Vortices of the Mediterranean Sea: An altimetric perspective. *J. Phys. Oceanogr.,* **36,** 87–103.

Isoguchi, O., and H. Kawamura, 2003: Eddies advected by time-dependent Sverdrup circulation in the western boundary of the subarctic North Pacific. *Geophys. Res. Lett.,* **30,** 1794, doi:10.1029/2003GL017652.

——, ——, and E. Oka, 2006: Quasi-stationary jets transporting surface warm waters across the transition zone between the subtropical and the subarctic gyres in the North Pacific. *J. Geophys. Res.,* **111,** C10003, doi:10.1029/2005JC003402.

Ito, S., and Y. Shimizu, 1997: Distribution patterns of temperature data and a method to draw isotherms in the Tohoku offshore area (in Japanese with English abstract). *Bull. Tohoku Natl. Fish. Res. Inst.,* **59,** 163–170.

Itoh, S., and T. Sugimoto, 2001: Numerical experiments on the movement of a warm-core ring with the bottom slope of a western boundary. *J. Geophys. Res.,* **106,** 26 851–26 862.

Iwao, T., M. Endoh, N. Shikama, and T. Nakano, 2003: Intermediate circulation in the northwestern North Pacific derived from subsurface floats. *J. Oceanogr.,* **59,** 893–904.

Jayne, S. R., and J. Marotzke, 2002: The oceanic eddy heat transport. *J. Phys. Oceanogr.,* **32,** 3328–3345.

Kawai, H., 1972: Hydrography of the Kuroshio Extension. *Kuroshio—Its Physical Aspects,* H. Stommel and K. Yoshida, Eds., University of Tokyo Press, 235–352.

Kitano, K., 1975: Some properties of warm eddies generated in confluence zone of Kuroshio and Oyashio Currents. *J. Phys. Oceanogr.,* **5,** 245–252.

Le Traon, P. Y., Y. Faugere, F. Hernandez, J. Dorandeu, F. Mertz, and M. Ablain, 2003: Can we merge *GEOSAT Follow-On* with TOPEX/Poseidon and *ERS-2* for an improved description of the ocean circulation? *J. Atmos. Oceanic Technol.,* **20,** 889–895.

McWilliams, J. C., and G. R. Flierl, 1979: Evolution of isolated, non-linear vortices. *J. Phys. Oceanogr.,* **9,** 1155–1182.

Mishra, P., S. Sainz-Trapaga, and T. Sugimoto, 1999: Evolution of Kuroshio warm-core ring 93A from hydrographicao propagation. *Ecosystem Dynamics of the Kuroshio–Oyashio Transition Region: Proceedings of the International Marine Science Symposium,* M. Terazaki et al., Eds., Japan Marine Science Foundation, 74–85.

Mizuno, K., and W. B. White, 1983: Annual and interannual variability in the Kuroshio Current system. *J. Phys. Oceanogr.,* **13,** 1847–1867.

Murakami, M., 1994: On long-term variations in hydrographic conditions in the Tohoku area (in Japanese with English abstract). *Bull. Tohoku Natl. Fish. Res. Inst.,* **56,** 47–56.

Okubo, A., 1970: Horizontal dispersion of floatable particles in vicinity of velocity singularities such as convergences. *Deep-Sea Res.,* **17,** 445–454.

Pascual, A., Y. Faugère, G. Larnicol, and P. Y. Le Traon, 2006: Improved description of the ocean mesoscale variability by combining four satellite altimeters. *Geophys. Res. Lett.,* **33,** L02611, doi:10.1029/2005GL024633.

Qiu, B., 2002: The Kuroshio Extension system: Its large-scale variability and role in the midlatitude ocean–atmosphere interaction. *J. Oceanogr.,* **58,** 57–75.

——, and S. M. Chen, 2005: Eddy-induced heat transport in the subtropical North Pacific from Argo, TMI, and altimetry measurements. *J. Phys. Oceanogr.,* **35,** 458–473.

Rio, M. H., and F. Hernandez, 2004: A mean dynamic topography computed over the World Ocean from altimetry, in situ measurements, and a geoid model. *J. Geophys. Res.,* **109,** C12032, doi:10.1029/2003JC002226.

Rogachev, K. A., 2000: Recent variability in the Pacific western subarctic boundary currents and Sea of Okhotsk. *Prog. Oceanogr.,* **47,** 299–336.

——, N. Shlyk, and E. Carmack, 2007: The shedding of mesoscale anticyclonic eddies from the Alaskan Stream and westward transport of warm water. *Deep-Sea Res. II,* **54,** 2643–2656.

Sainz-Trápaga, S. M., and T. Sugimoto, 1998: Spreading of warm water from the Kuroshio Extension into the perturbed area. *J. Oceanogr.,* **54,** 257–271.

——, G. J. Goni, and T. Sugimoto, 2001: Identification of the Kuroshio Extension, its bifurcation and northern branch from

altimetry and hydrographic data during October 1992–August 1999: Spatial and temporal variability. *Geophys. Res. Lett.,* **28,** 1759–1762.

Shimizu, Y., and S. Ito, 1996: A new method to draw isotherms in the Tohoku offshore area—New interpolation method ''flexible Gaussian filter.'' *Bull. Tohoku Natl. Fish. Res. Inst.,* **58,** 105–117.

Smith, W. H. F., and D. T. Sandwell, 1997: Global sea floor topography from satellite altimetry and ship depth soundings. *Science,* **277,** 1956–1962.

Suga, T., and K. Hanawa, 1990: The mixed-layer climatology in the northwestern part of the North Pacific Subtropical Gyre and the formation area of Subtropical Mode Water. *J. Mar. Res.,* **48,** 543–566.

Sugimoto, T., and H. Tameishi, 1992: Warm-core rings, streamers and their role on the fishing ground formation around Japan. *Deep-Sea Res.,* **39,** S183–S201.

Tomosada, A., 1986: Generation and decay of Kuroshio warm-core rings. *Deep-Sea Res.,* **33,** 1475–1486.

van Leeuwen, P. J., 2007: The propagation mechanism of a vortex on the beta plane. *J. Phys. Oceanogr.,* **37,** 2316–2330.

Verron, J., and C. Le Provost, 1991: Response of eddy-resolved general-circulation numerical-models to asymmetrical wind forcing. *Dyn. Atmos. Oceans,* **15,** 505–533.

Weiss, J., 1991: The dynamics of enstrophy transfer in 2-dimensional hydrodynamics. *Physica D,* **48,** 273–294.

Yasuda, I., 2003: Hydrographic structure and variability in the Kuroshio–Oyashio transition area. *J. Oceanogr.,* **59,** 389–402.

——, K. Okuda, and K. Mizuno, 1986: Numerical study on the vortices near boundaries: Considerations on warm-core rings in the vicinity of east coast of Japan (in Japanese with English abstract). *Bull. Tohoku Reg. Fish. Res. Inst.,* **48,** 67–86.

——, ——, M. Hirai, Y. Ogawa, H. Kudoh, S. Fukushima, and K. Mizuno, 1988: Short-term variations of the Tsugaru Warm Current in autumn (in Japanese with English abstract). *Bull. Tohoku Reg. Fish. Res. Inst.,* **50,** 153–191.

——, ——, and ——, 1992: Evolution of a Kuroshio warm-core ring—Variability of the hydrographic structure. *Deep-Sea Res.,* **39,** S131–S161.

——, ——, and Y. Shimizu, 1996: Distribution and modification of North Pacific intermediate water in the Kuroshio–Oyashio interfrontal zone. *J. Phys. Oceanogr.,* **26,** 448–465.

——, and Coauthors, 2000: Cold-core anticyclonic eddies south of the Bussol' Strait in the northwestern subarctic Pacific. *J. Phys. Oceanogr.,* **30,** 1137–1157.